TANGENTIAL DISCONTINUITIES IN THE SOLAR WIND

by

James Marshall Turner

Center for Space Research
Massachusetts Institute of Technology
Cambridge, Massachusetts 02139

CSR-P-71-59 May 1971

CENTER FOR SPACE RESEARCH
MASSACHUSETTS INSTITUTE OF TECHNOLOGY

Submitted to JGR May 1971

TANGENTIAL DISCONTINUITIES IN THE SOLAR WIND

by

James Marshall Turner

Center for Space Research
Massachusetts Institute of Technology
Cambridge, Massachusetts 02139

CSR-P-71-59 May 1971

Abstract

Solar wind plasma and magnetic field data were used to identify tangential discontinuities during the first 40 days of the flight of Mariner 5. The normals to the tangential discontinuity surfaces had a strongly preferred orientation which was in the ecliptic plane and perpendicular to the spiral field direction. Tangential discontinuities have the property that the magnetic field on both sides of the discontinuity and the change in velocity across the discontinuity are confined to the plane of the discontinuity. For quiet plasma streams both the magnetic field and velocity showed strong evidence of this confinement away from the discontinuity as indicated by the fact that the least likely directions of changes in $\underline{B}$ and $\underline{V}$ near the discontinuity tended to be distributed along the normal to the discontinuity surface. In disturbed plasma streams, the magnetic field also behaved as it did in the quiet stream case, while the velocity confinement in this case was only true at the discontinuity and did not persist away from the discontinuity. The least likely directions of change for the magnetic field and velocity near the discontinuities were different from the least likely directions found overall for the 40 days studied.

I. Introduction

In this paper, tangential discontinuities in the solar wind are studied to determine if there are preferred directions in their orientations and if there are differences between the overall solar wind flow and the flow near the discontinuities.

Tangential discontinuities have been observed previously. Burlaga and Ness' (1969) analysis of Pioneer 6 and IMP 3 magnetic field and plasma data, with most of the emphasis on the magnetic field, resulted in one set of observations. Siscoe et al. (1969b) used plasma and magnetic field data from Pioneer 6 on equal footing and showed that the data were consistent with the presence of tangential discontinuities. Definite confirmation was not possible since the plasma velocity component out of the ecliptic plane was not reliable. Siscoe and Coleman (1969) found tangential discontinuities with Mariner 4, and like Burlaga and Ness they relied primarily on magnetic field data. All three groups found that the tangential discontinuities observed or suspected tended to orient themselves on the whole along the spiral field direction at the location of the spacecraft; however, individual events may deviate from this orientation. Siscoe et al. (1969b) referred to this effect as an east-west asymmetry in the orientation. Siscoe and Coleman also reported that the tangential discontinuity orientations had a sector dependent north-south asymmetry with respect to the ecliptic plane.

The approach in this paper is similar to that of Siscoe et al. (1969b) in the sense that plasma and magnetic field data are used on an equal basis in identifying tangential discontinuities. In addition, the plasma data used here are reliable for all three velocity components.

II. The Experiment

The Mariner 5 spacecraft was launched June 14, 1967 toward an encounter with Venus. The period of interest in this paper is the first forty days of the flight because this was the time when the data acquisition rate was the highest.

A satellite centered RTN coordinate system was used: the R direction is radially outward from the sun, the T direction is parallel to the solar equatorial plane and positive in the direction of planetary motion, the N direction is directed northward along $\underline{R} \times \underline{T}$. The RT plane and the ecliptic plane are only a few degrees apart and thus are essentially the same.

Magnetic field measurements were made by a low-field vector helium magnetometer (Connor, 1968); three vector field readings were obtained every 12.6 seconds for the first forty days and every 50.4 seconds after that. The plasma detector, a modulated grid Faraday cup (Lazarus et al. 1967) pointed at the sun and measured positive ion currents in 32 energy levels from 40 to 9400 ev, with samples taken every 5.04 minutes at the high data rate.

The magnetic field data considered in the following analysis were 5.04 minute averages of the 12.6 second readings to make the magnetic field and plasma data comparable in time. The plasma parameters were obtained by fitting an isotropic Maxwellian distribution to the data. The uncertainties in the parameters are 10% in density, 1% in the radial component of the wind velocity, V_R, $\frac{1}{2}^\circ$ in the flow direction resulting in an uncertainty of $\frac{\pi}{360}$ (i.e. $\frac{1}{2}^\circ$ converted into radians) x V_R for V_T and V_N and a few tenths of a gamma in the magnetic field components.

III. Identification of Tangential Discontinuities

Identification of tangential discontinuities was made by requiring that five conditions be met. Conditions one, four, and five deal with the physical properties of tangential discontinuities while conditions two and three optimize the reliability of the plasma and magnetic field values which characterize the solar wind on both sides of the discontinuity.

The first condition was that there had to be a 20% or more change in density between consecutive data points. Although a change in density is not necessary for tangential discontinuities, the condition was imposed to eliminate all rotational discontinuities.

The second condition was a steady state requirement to insure that the plasma and magnetic field parameters used in the analysis were representative of the solar wind on both sides of the discontinuity. If a,b,c,d,e,f were

consecutive data points with the 20% or more change in density occurring between points c and d, then it was demanded that the plasma and field values associated with points a,b, and c not change within subjectively defined limits (usually about 10%) from point to point and similarly for d,e, and f. If this requirement was satisfied, data from points b and e were used to represent the pre- and post-discontinuity solar wind. The steady state requirement insured that these two points reliably characterized the two solar wind states, since the solar wind sample which was used to compute the parameters of these two points was entirely on one side of the discontinuity. That is, since the discontinuity occurred between c and d it is not known for example how much of the sample used by point c contained pre-discontinuity plasma, but the plasma for point b must have all come from the pre-discontinuity plasma. In all, 82 cases satisfied conditions one and two.

The third condition, like the second, was taken to optimize the accuracy of the analysis. It is a property of tangential discontinuities that $\underline{B}_1$ and $\underline{B}_2$ (the pre- and post- discontinuity magnetic fields) must lie in the plane of the discontinuity. Thus $\hat{n} = \underline{B}_1 \times \underline{B}_2 / (|\underline{B}_1 \times \underline{B}_2|)$ is a unit vector normal to the discontinuity plane. Hence if $\underline{B}_1$ and $\underline{B}_2$ are very nearly parallel or antiparallel, $\hat{n}$ is not very well determined. The third condition insures that $\underline{B}_1$ and $\underline{B}_2$ are sufficiently separated so that the uncertainty in $\hat{n}$ is reduced. For each 5.04 minute average of the magnetic field a standard deviation over the averaging period was computed for each component. Let

σ_1 be the largest of the three standard deviations computed for point b and let σ_2 be similarly defined for point e. Let $3\sigma/|\underline{B}|$ be the greater of $3\sigma_1/|\underline{B}_1|$ and $3\sigma_2/|\underline{B}_2|$. It was required that $\sin^{-1}(3\sigma/|\underline{B}|) < \cos^{-1}(\underline{B}_1 \cdot \underline{B}_2/(|\underline{B}_1||\underline{B}_2|))$. It was found that 38 cases satisfied conditions one, two, and three.

The fourth condition was that there must be pressure balance across the discontinuity. If α-particles are ignored, electron isotropy assumed and a proton pressure anisotropy introduced, the pressure equation can be written as

$$kT_{e_2} = (n_1/n_2)kTe_1 + \xi((n_1/n_2)kT_{p_1} + kT_{p_2}) + (B_1^2 - B_2^2)/8\pi n_2$$

where the pre- and post-discontinuity proton and electron temperatures are denoted by the proper subscript, n is the proton number density, and $\xi \equiv 1 - 4\pi(P_{\parallel} - P_{\perp})/B^2$ is the anisotropy factor. It was found that ξ varied between 0.7 and 1.0 (see Hundhausen et al.,1970 for proton anisotropy) and that the electron temperature, T_e, is generally $10^5 °K \leq T_e \leq 2 \times 10^5 °K$ (see e.g., Montgomery et al.,1968). Both limits for the usual electron temperature range were substituted for T_{e_1} and T_{e_2} was computed for both cases. This was done for a series of ξ's from 0.7 to 1.0. Cases which had unreasonable values of T_{e_2} were to be eliminated. Of the 38 events still being considered at this stage, 36 had one or more values of T_{e_2} within the typical electron temperature range previously mentioned and thus were consistent with pressure balance across the discontinuity.

The fifth and final condition, which is a property of tangential discontinuities, required that there be no flow across the discontinuity plane. This would mean that $\Delta\underline{V} \cdot \hat{n} = 0$ where $\Delta\underline{V}$ is the change in velocity from the pre- to post-discontinuity

value and $\hat{n}$ is the unit normal previously defined. Only cases with $|\Delta\underline{V} \cdot \hat{n}| < 8$ km/sec were considered acceptable since 8 km/sec is on the order of the uncertainty of $\Delta\underline{V}$. Of the 36 remaining cases, 35 satisfied this condition.

Data from a typical event is shown in Figure 1.

IV. Matrix Technique

The major portion of the analysis of the data utilized a matrix technique for determining the distribution of a set of vectors. Consider a set of N measurements of a vector $\underline{A}$. The real, symmetric matrix $T_{\ell m} = \sum_{k=1}^{N} A_\ell^{(k)} A_m^{(k)}$ can be formed where $A_\ell^{(k)}$ is the ℓth component of the kth vector. The three orthonormal eigenvectors of the matrix give an indication of the preferred directions of the set of vectors. The strength of the preference can be found by computing $\varepsilon_i^2 = \sum_{k=1}^{N} (\hat{A}^{(k)} \cdot \hat{e}_i)^2$, (i=I,II,III) where $\hat{A}^{(k)} = \underline{A}^{(k)} / |\underline{A}^{(k)}|$ and $\hat{e}_i$ is one of the three eigenvectors. Thus an isotropic distribution would yield $\varepsilon_I^2 = \varepsilon_{II}^2 = \varepsilon_{III}^3$ On the other extreme, if all the vectors were along the $\hat{e}_I$ direction, this distribution would make $\varepsilon_I^2 = N$, $\varepsilon_{II}^2 = \varepsilon_{III}^2 = 0$.

It should be noted that in the discussion which follows ε_I will be associated with the eigenvector around which the $\underline{A}^{(k)}$ most tend to cluster, while ε_{III} will be associated with the eigenvector around which there is the least tendency to cluster.

V. Discussion of Results

1. Orientation of Tangential Discontinuities

The 35 tangential discontinuities were observed to occur at random throughout the 40 days with no obvious pattern. That is, they occurred during both high and low velocity solar wind streams and in the transition regions between them.

The tangential discontinuity normals, $\hat{n}$, have a strongly favored orientation. This can be seen with the help of Figure 2 in which the normals are plotted in a polar coordinate system with the R-axis taken as the polar axis. It is evident that the favored orientation of $\hat{n}$ is in the RT plane and nearly perpendicular to the spiral field direction. In addition $\hat{n}$ generally has a small component out of the RT plane but does not have a preferential north or south orientation. Not only were there as many northward directed normals as southward, but also there were no sustained intervals of time when one orientation dominated. These results for the preferential orientation of $\hat{n}$ are confirmed by applying the matrix technique to the set of normals. Table 1 lists the RTN components of each eigenvector along with the polar angle, θ, and an azimuthal angle, ϕ, which is measured in the TN plane with $\phi=0°$ corresponding to the positive T direction and $\phi=90°$ corresponding to the positive N direction. In addition ε_i^2 (i=I,II,III) and a normalization factor ε_i^2/N, where N is the number of events, are given. The most favored eigenvector $\hat{e}_I^n$ is

nearly perpendicular to the spiral field direction and slightly tilted out of the RT plane. In Figure 3, $\hat{e}_I^n$ is plotted in the same polar coordinate system used in Figure 2 and is denoted by an open circle O. It should be noted that the magnetic field averaged over the 40 days is very close to the theoretical spiral field direction: the RTN components in gammas of the average field are (-1.86, 1.67, 0.05).

The east-west asymmetry in the orientation of the discontinuity planes agrees with the previously mentioned observations from other spacecrafts. In addition, it is also in agreement with the general east-west asymmetry in the solar wind which was demonstrated by Siscoe et al. (1969a), namely, that the faster plasma streams tend to come from a more westerly direction than the slower streams.

2. Behavior of the Solar Wind Near Tangential Discontinuities

In order to study what happened away from the immediate vicinity of a discontinuity each day was divided into eight three hour segments with the first three hours being in the first segment etc. The point-by-point changes in $\underline{B}$ and $\underline{V}$ were computed within each segment and the matrix technique applied. The result of this was a set of eigenvectors denoting the directions along which $\underline{B}$ was most likely to change, least likely to change, and an intermediate direction. There was a similar result for $\underline{V}$. In order to be used in further analysis,

two conditions had to be met. First, a segment had to contain at least half the maximum number of data points; second, $\varepsilon^2_{III} \leq \frac{2}{3} \varepsilon^2_{II}$ to insure that there was a clear-cut direction along which $\underline{B}$ or $\underline{V}$ was least likely to change during the segment. There were 320 segments in all, of which 236 met the two conditions for $\underline{B}$ and 197 for $\underline{V}$.

The next step was to apply the matrix technique again but this time to the set of directions of least likely change in $\underline{B}$ from each of the 236 segments and similarly for the 197 segments for $\underline{V}$. The results were directions of least likely change for $\underline{B}$ and $\underline{V}$ which characterized the 40 days. The results are summarized in Table 2 with the least favored directions for change in $\underline{B}$, $\hat{e}_I^B$, and in $\underline{V}$, $\hat{e}_I^V$, being plotted in Figures 3 and 4 respectively and denoted by $\boxtimes$ in both cases. The result for $\underline{V}$ as reflected by $\hat{e}_I^V$ demonstrates the general east-west asymmetry previously mentioned since it indicates that there are few changes in $\underline{V}$ in which ΔV_R and ΔV_T have the same sign. The result for $\underline{B}$ indicates that the RTN coordinate system essentially coincides with the principal coordinate system for the magnetic field, i.e. the eigenvectors associated with measurements of changes in $\underline{B}$ are almost parallel to the RTN axes. It is not clear if the result for $\underline{B}$ is real or a spurious conclusion affected by the method of analysis. If the result is real it is not certain what the interpretation of it would be.

To determine the behavior of the solar wind near tangential discontinuities, the matrix technique was applied only to those acceptable segments containing tangential discontinuities. There were 30 segments for $\underline{B}$ and 23 for $\underline{V}$. It was found that indeed the magnetic field condition at the discontinuity, i.e. $\underline{B} \cdot \hat{n} = 0$, persisted for some distance from the discontinuity as shown by the fact that the least likely direction of change of $\underline{B}$ is only a few degrees from the most favored direction of the tangential discontinuity normals (see Table 3). It should be noted from ϵ_i^2/N that this is a rather strong effect. The most favored eigenvector, $\hat{e}_I^{B'}$ is plotted in Figure 3 and denoted by *.

There was a different result, however, for the velocity. If the 23 segments for $\underline{V}$ are subdivided into quiet stream and disturbed stream segments, two opposite effects occur. The basis for the distinction was the hourly average of bulk velocity. If the differences in the hourly averages of the bulk velocity during the segment were 2-5 km/sec, it was considered a quiet stream or small variation segment. If the differences in the hourly averages were $\geq$ 10 km/sec, it was considered a disturbed stream or large variation segment. Thus the $\underline{V}$ segments fell into two classes:

(a) small variation - 6 segments
(b) large variation - 17 segments

The results for each subdivision along with that for all 23 segments are shown in Table 4. As indicated by $\hat{e}_I^{V_a}$, the $\Delta V \cdot \hat{n}$ condition at the discontinuity seems to persist back into the plasma for the quiet streams, similar to the behavior of

the magnetic field. However, for disturbed streams, this condition is totally wiped out by the rapid and large scale changes in the bulk velocity. Both $\hat{e}_I V_a$ and $\hat{e}_I V_b$ are plotted in Figure 4 in addition to $\hat{e}_I V'$ and are denoted by *,+, and • respectively.

The magnetic field and velocity behavior is quite different near tangential discontinuities than is the case overall. For the 40 days the least likely direction of change in $\underline{B}$ is along the R-direction; however, near tangential discontinuities the least likely direction for change was the same as the normal to the discontinuity. The quiet stream result for $\underline{V}$ was very similar to the 40 day result. A difference came about from the disturbed streams near tangential discontinuities and this was significantly different from the 40 day result. For disturbed streams the least likely direction is in the TN plane.

VI. Conclusion

1. There is a strongly favored direction for the orientation of tangential discontinuity normals. The direction is perpendicular to the spiral field direction and predominantly near the ecliptic plane in agreement with other observations. There was no evidence of a north-south asymmetry, however.

2. The magnetic field some distance away from the discontinuity still appears to be confined to the same plane in which it was confined at the discontinuity.
3. For quiet streams, the changes in velocity away from the discontinuity also tend to be confined to the same plane in which changes were confined at the discontinuity.
4. For disturbed streams, the changes in velocity away from the discontinuity are not confined to the same plane in which changes were confined at the discontinuity.
5. The least likely direction of change in $\underline{B}$ during the 40 days under study is along the R-direction while near tangential discontinuities the least likely direction is coupled with the discontinuity orientation as mentioned in the second conclusion. For quiet plasma streams, near tangential discontinuities, the least likely direction of change in $\underline{V}$ is very similar to that for the 40 days. The disturbed streams have a least likely direction of change which is predominantly in the TN plane as would be expected since V_R is changing by large amounts in these cases.

Table 1: Eigenvectors for the Distribution of $\hat{n}$

	R	T	N	θ	ϕ	ε_i^2	ε_i^2/N
$\hat{e}_I^n$	.820	-.552	-.150	35°	335°	18.029	.515
$\hat{e}_{II}^n$	.018	.237	.971	89°	76°	10.162	.290
$\hat{e}_{III}^n$	-.572	.880	-.184	145°	348°	6.810	.195

Table 2: Eigenvectors for the Least Likely Direction for Changes in B and V for the Entire 40 Days

	R	T	N	θ	φ	ε_i^2	ε_i^2/N	
$\hat{e}_I^V$	.836	.532	.132	33°	14°	93.093	.473	
$\hat{e}_{II}^V$	-.523	.702	.483	122°	35°	57.158	.290	(N=197)
$\hat{e}_{III}^V$	.165	-.473	.865	71°	119°	46.747	.237	
$\hat{e}_I^B$	.993	-.079	-.086	7°	227°	109.699	.465	
$\hat{e}_{II}^B$	.096	.971	.220	84°	13°	70.154	.297	(N=236)
$\hat{e}_{III}^B$	.066	.226	.972	86°	103°	54.143	.229	

Table 3: Eigenvectors for the Least Likely Direction of Change in $\underline{B}$ in Segments Containing Tangential Discontinuities

	$\underline{R}$	$\underline{T}$	$\underline{N}$	$\underline{\theta}$	$\underline{\phi}$	$\underline{\varepsilon_i^2}$	$\underline{\varepsilon_i^2/N}$	
$\hat{e}_I^{B'}$	.735	.676	.055	43°	5°	15.024	.501	
$\hat{e}_{II}^{B'}$	-.676	.737	-.011	133°	359°	8.586	.286	(N=30)
$\hat{e}_{III}^{B'}$	-.048	-.029	.998	93°	92°	6.390	.213	

Table 4: Eigenvectors for the Least Likely Direction of Change in $\underline{V}$ for Segments Containing Tangential Discontinuities

	R	T	N	θ	φ	ε_i^2	ε_i^2/N	
$\hat{e}_I^{V_a}$	.881	.465	.088	28°	11°	3.604	.601	
$\hat{e}_{II}^{V_a}$	-.453	.882	-.126	117°	352°	1.818	.302	(N=6)
$\hat{e}_{III}^{V_a}$	-.137	.071	.988	98°	86°	0.579	.097	
$\hat{e}_I^{V_b}$	.121	.726	.677	83°	43°	9.135	.537	
$\hat{e}_{II}^{V_b}$	.708	.415	-.572	45°	306°	5.281	.311	(N=17)
$\hat{e}_{III}^{Vb}$	.696	-.549	.464	46°	120°	2.584	.172	
$\hat{e}_I^{V'}$	.388	.794	.468	63°	31°	11.241	.489	
$\hat{e}_{II}^{V'}$	-.773	.004	.635	131°	90°	7.408	.322	(N=23)
$\hat{e}_{III}^{V'}$	.502	-.608	.615	60°	135°	4.354	.189	

References

Burlaga, L.F. and N.F. Ness, Tangential discontinuities in the solar wind, Solar Phys., 9, 467, 1969.

Colburn, D.S. and C.P. Sonett, Discontinuities in the solar wind, Space Sci. Rev., 5, 439, 1966.

Connor, B.V., Space magnetics: Mariner 5 magnetometer experiment, IEEE Trans. Magnetics, Mag-4, 391, 1968.

Hundhausen, A.J., S.J. Bame, J.R. Asbridge, and S.J. Sydoriak, Solar wind properties: Vela 3 observations from July, 1965 to June, 1967, J. Geophys. Res., 75, 4643, 1970.

Lazarus, A.J., H.S. Bridge, J.M. Davis, and C.W. Snyder, Initial results from the Mariner 5 plasma experiment, Space Res., 7, 1296, 1967.

Montgomery, M.A., S.J. Bame, and A.J. Hundhausen, Solar wind electrons: Vela 4 measurements, J. Geophys. Res., 73, 4999, 1968.

Siscoe, G.L., and P.J. Coleman, On the north-south asymmetry in the solar wind, Solar Phys., 8, 415, 1968.

Siscoe, G.L., L. Davis Jr., P.J. Coleman, Jr., E.S. Smith, and D.E. Jones, Power spectra and discontinuities of the interplanetary magnetic field: Mariner 4, J. Geophys. Res., 73, 61, 1968.

Siscoe, G.L. B. Goldstein, and A.J. Lazarus, An east-west asymmetry in the solar wind velocity, J. Geophys. Res., 74, 1759, 1969a.

Siscoe, G.L., J.M. Turner, and A.J. Lazarus, Simultaneous plasma and magnetic field measurements of probable tangential discontinuities in the solar wind, Solar Phys. 6, 456, 1969b.

Acknowledgement

I am grateful to Dr. E.J. Smith of the Jet Propulsion Laboratory, Drs. Leverett Davis, Jr. and J.W. Belcher of the California Institute of Technology, Dr. P.J. Coleman, Jr. of the University of California at Los Angeles and Dr. D.E. Jones of Brigham Young University for providing me with the magnetic field data from Mariner 5. I would also like to thank Dr. A.J. Lazarus of the Massachusetts Institute of Technology for the Mariner 5 plasma data. I am grateful also for the fruitful discussions which I had with Professors S. Olbert, G.L. Siscoe and V.M. Vasyliunas.

This work is supported in part by the National Aeronautics and Space Administration under Contract NGL-22-009-015.

Figure Captions

Figure 1: In this figure data from a typical tangential discontinuity are plotted. The data include the bulk velocity, positive ion number density, proton thermal speed, solar equatorial polar angle, solar equatorial longitude, and the magnitude of the magnetic field.

Figure 2. This is a polar plot of the tangential discontinuity normals. The R-axis is chosen as the polar axis. Since all normals are taken to point outward, i.e. to have positive R-components, the polar angle, θ, ranges from 0° to 90°. The other angle in the figure, ϕ, is measured in the TN plane with ϕ = 0° corresponding to the positive T direction and ϕ = 90° being the positive N-direction. The angle θ is measured outward from the center of the plot while ϕ is in the plane of the plot and increases clockwise.

Figure 3. This is a polar plot of some of the eigenvectors found in the Tables. The angles θ and ϕ are defined as they were in Figure 2. The eigenvectors plotted, the Tables in which they are found, and the symbol used to designate them are:

e_I^n	Table 1	0
e_I^β	Table 2	$\boxed{x}$
$e_I^{\beta'}$	Table 3	*

Figure 4. This figure is similar to Figure 3, but with the velocity eigenvectors plotted. The eigenvectors presented are:

e_I^n	Table 1	0
e_I^V	Table 2	⊠
$e_I^{V_a}$	Table 4	*
$e_I^{V_b}$	Table 4	+
$e_I^{V'}$	Table 4	●

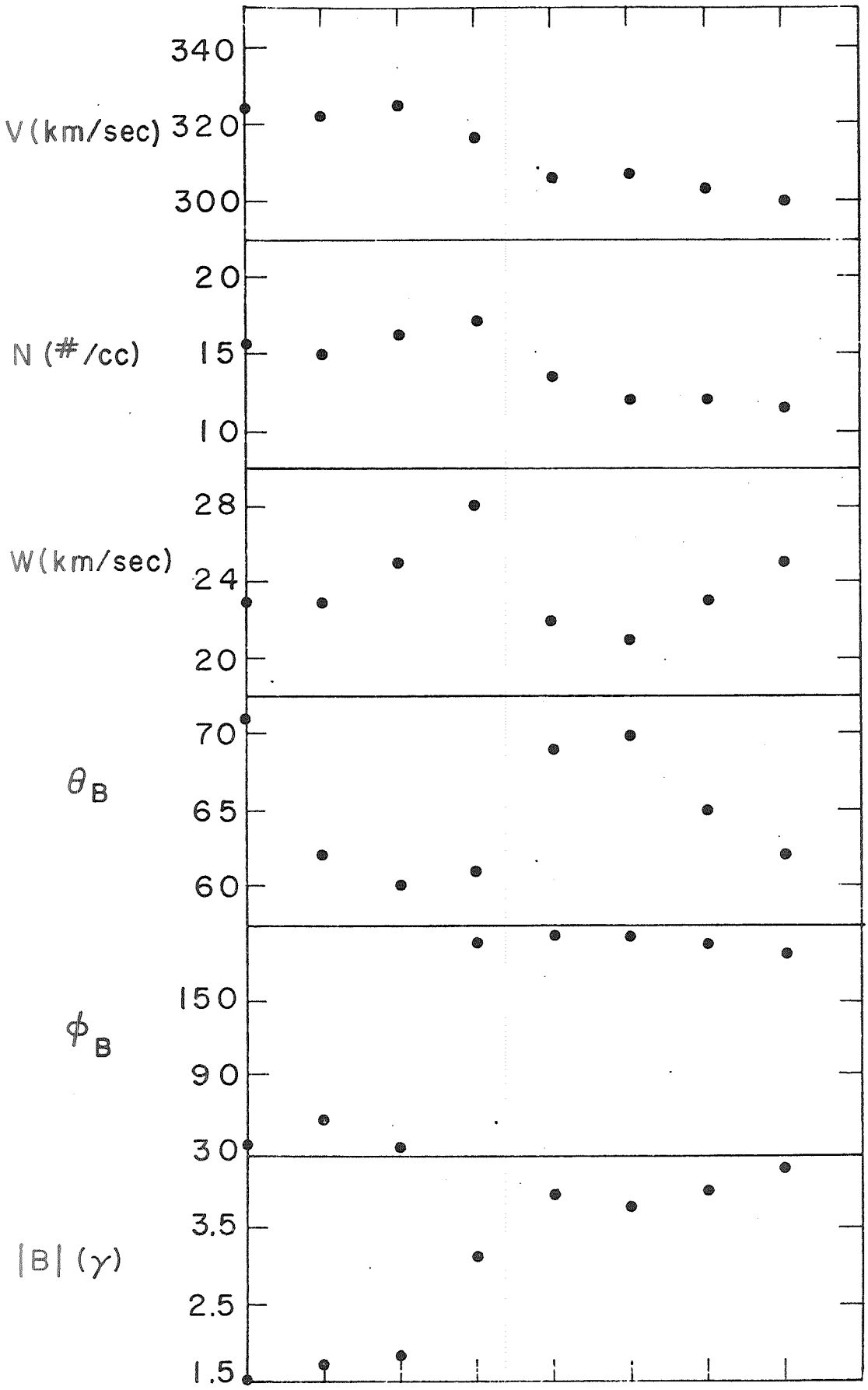
340
320
300
V(km/sec)
20
15
10
N (#/cc)
28
24
20
W(km/sec)
70
65
60
θ_B
150
90
30
ϕ_B
3.5
2.5
1.5
|B| (γ)
450 455 500 505 510 515 520 525
UT

FIGURE 1

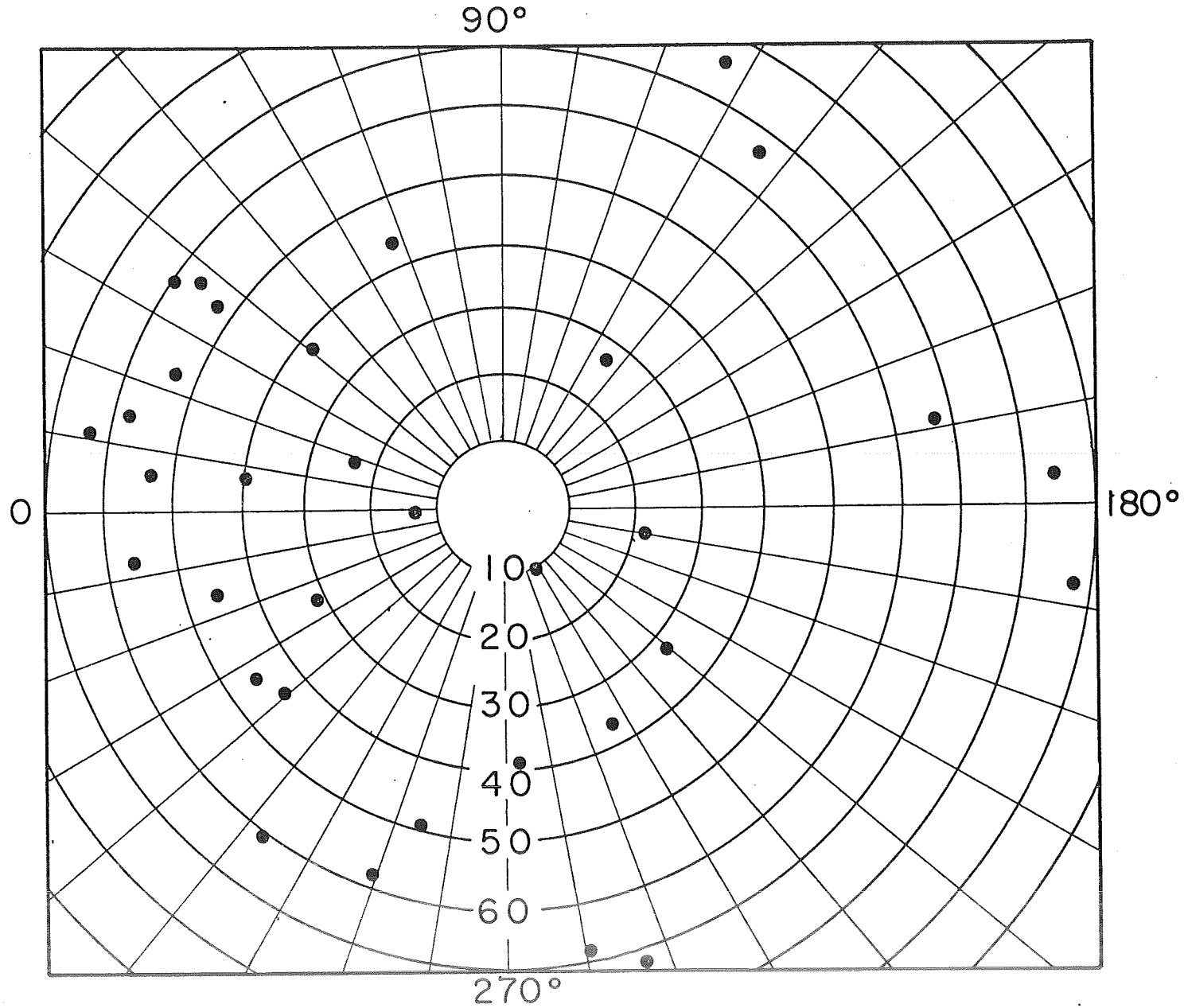

FIGURE 2

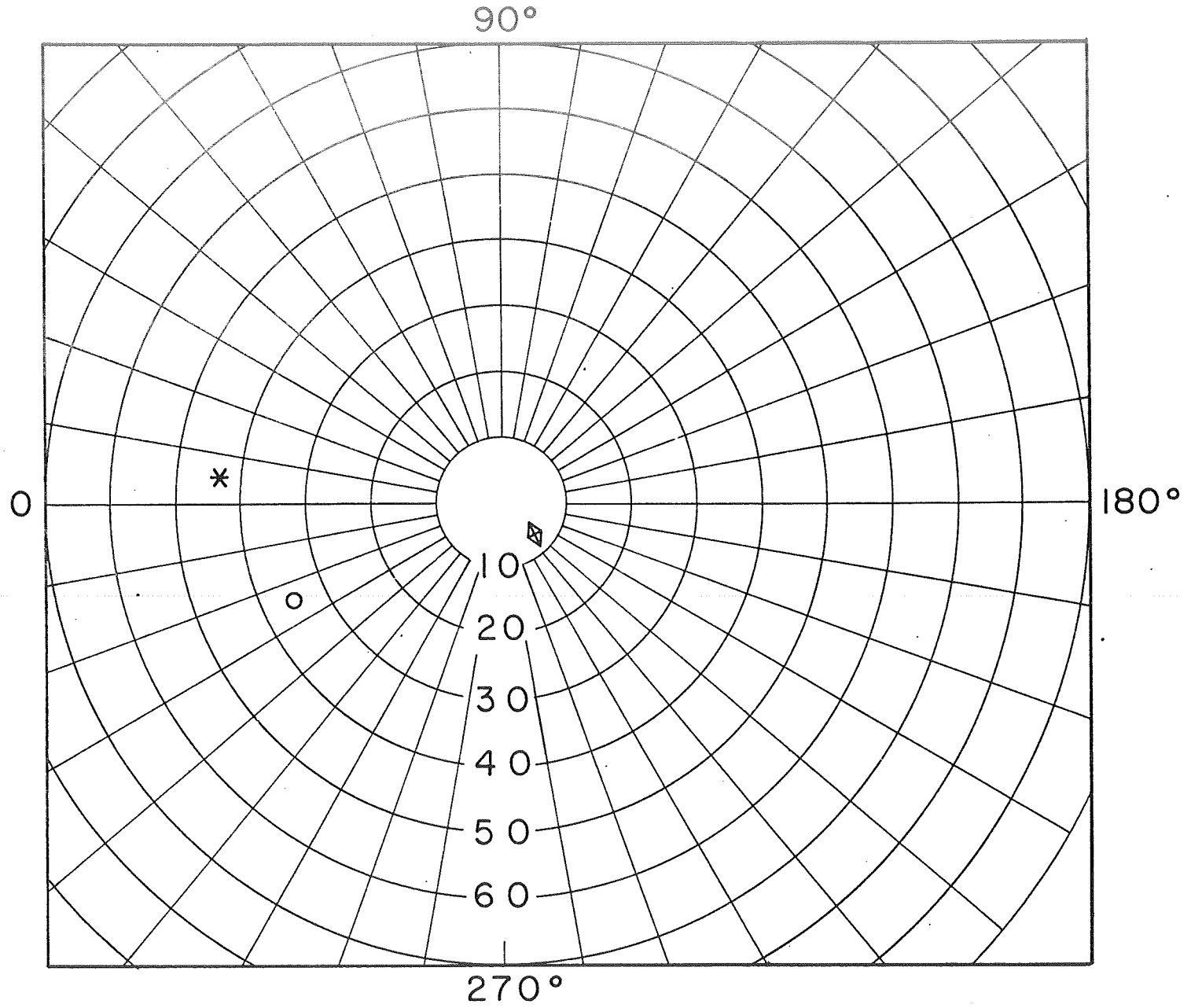

FIGURE 3

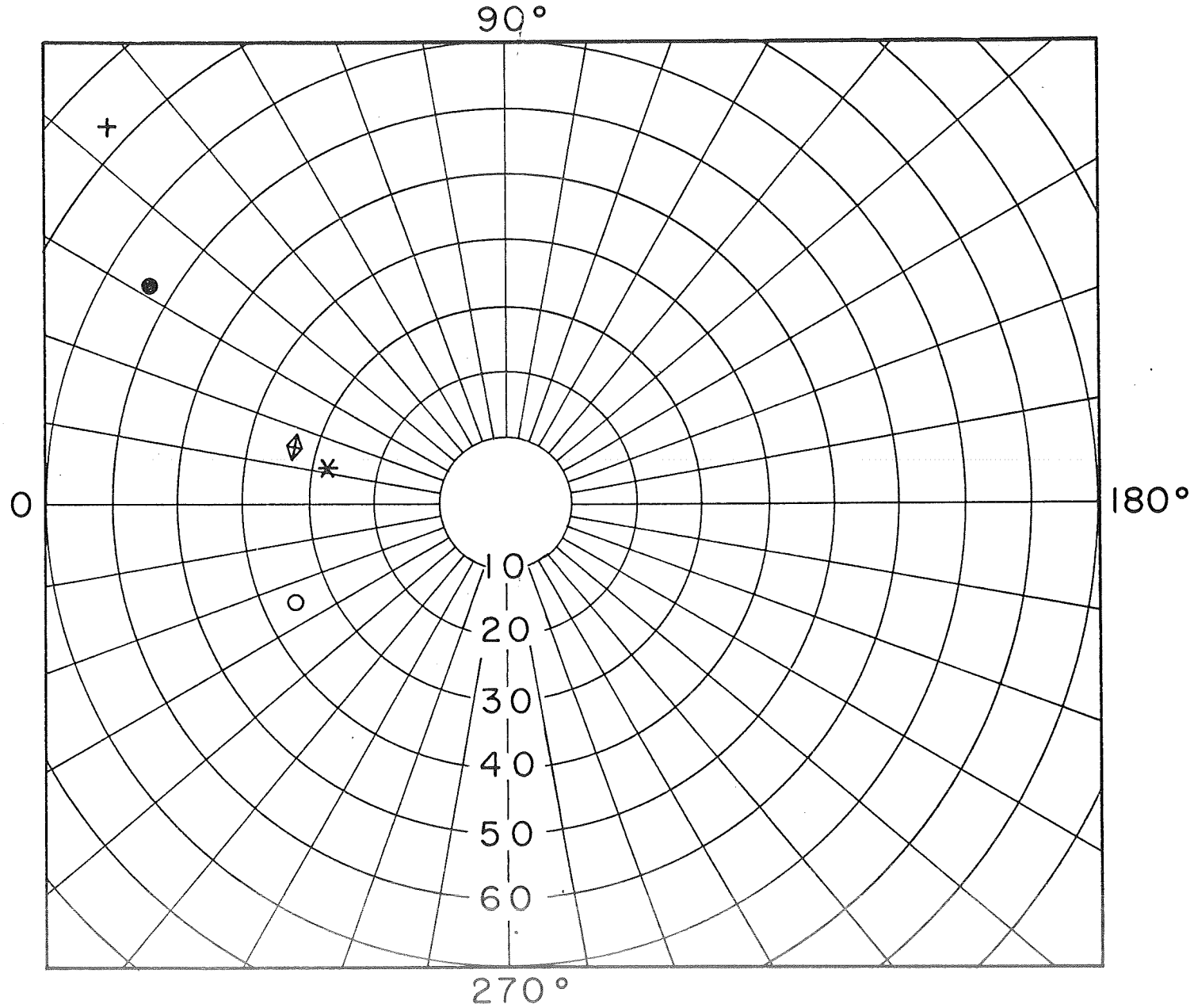

FIGURE 4